Wide-Gap $Zn_{1-x}Ni_xO$ Alloy: A Transparent *p*-Type Oxide

Chao Ping Liu,[1,2] Kingsley O. Egbo,[3] Chun Yuen Ho,[3] Ying Wang,[3] Cong Kang Xu,[1,2] and Kin Man Yu[3,4,*]

[1] *Research Center for Advanced Optics and Photoelectronics, Department of Physics, College of Science, Shantou University, Shantou, Guangdong 515063, China*

[2] *Key Laboratory of Intelligent Manufacturing Technology of MOE, Shantou University, Shantou, Guangdong 515063, China*

[3] *Department of Physics, City University of Hong Kong, 83 Tat Chee Avenue, Kowloon, Hong Kong*

[4] *Department of Materials Science and Engineering, City University of Hong Kong, 83 Tat Chee Avenue, Kowloon, Hong Kong*

(Received 5 December 2019; revised manuscript received 22 January 2020; accepted 3 February 2020; published 19 February 2020)

The development of transparent bipolar oxide devices is largely hampered by the lack of oxides with reliable *p*-type conductivity. Recent calculations show that rock salt (RS) structured ZnO alloys are promising candidates for transparent *p*-type oxides. Here, we synthesize wide-gap $Zn_{1-x}Ni_xO$ alloy thin films over the entire composition range on glass substrates by means of radiofrequency magnetron sputtering. We find that the $Zn_{1-x}Ni_xO$ alloy thin films undergo a phase transition from wurtzite (WZ) to RS structure as the Ni content x increases to $x \sim 0.27$. Interestingly, the band gap of RS-$Zn_{1-x}Ni_xO$ is about 4.6 eV at the WZ to RS transition composition ($x \sim 0.27$) and decreases with x to the value of RS-NiO ($\sim$3.8 eV). Nominally undoped alloy thin films sputtered in pure Ar are semi-insulating, while O-rich RS-$Zn_{1-x}Ni_xO$ thin films with relatively high x (e.g., $x \geq 0.5$) sputtered in Ar^+ 1.4% O_2 and/or with Cu doping exhibit good *p*-type conductivity at room temperature. The hole transport in these RS-$Zn_{1-x}Ni_xO$ alloy thin films follows a small polaron hopping process, with activation energy ranges from 0.19 to 0.32 eV. Drastic differences in the electronic band structure of the WZ and RS $Zn_{1-x}Ni_xO$ alloys are also observed with a type II band offset for alloys at the WZ to RS transition composition. The valence band maximum (VBM) of the RS phase is >1 eV above that of the WZ phase, making them energetically more favorable for the formation of native acceptor defects. The much higher VBM position of RS alloys also favors their extrinsic *p*-type doping efficiency.

DOI: 10.1103/PhysRevApplied.13.024049

I. INTRODUCTION

Wide-gap transition-metal oxides have attracted much attention in recent years, owing to their technological importance in a broad range of optoelectronics applications, including solar cells, photodetectors, and light-emitting diodes (LEDs) [1–3]. However, the development of oxide-based optoelectronics is largely hindered by the lack of reliable *p*-type metal oxides. For instance, high-efficiency WZ-ZnO-based ultraviolet LEDs have not been realized due to difficulties in achieving robust *p*-type ZnO with controlled electrical properties [4–6]. For an ideal transparent *p*-type oxide, the material has to have a wide gap with a high valence band edge (VBE) and low hole effective mass. In most metal oxides, however, the VBE states are derived from O 2*p* orbitals and located far below the vacuum level, resulting in localization of holes (formation of deep acceptor states), and thus, making efficient *p*-type doping of these materials (including WZ-ZnO) extremely challenging [7]. In the last decade, numerous experimental and theoretical investigations have been devoted to the design and development of various *p*-type metal oxides through VB engineering [7–12]. For example, Hautier *et al*. identified a few wide-gap *p*-type metal oxides (e.g., $A_2Sn_2O_3$, A = K, Na) with exceptionally low hole effective mass based on high-throughput computations [11]. In our recent work, we demonstrated that the VB maximum (VBM) of the ZnO-rich highly mismatched alloy WZ-$ZnO_{1-x}Te_x$ shifted upward by about 1 eV due to the anticrossing interaction between the VB states of the matrix, ZnO, and Te localized states, making it more favorable for *p*-type doping compared with other transition-metal oxides [12].

A recent computational study by Goyal and Stevanović proposed that ZnO in the RS phase could be a promising *p*-type wide-gap oxide, with a relatively high absolute VBE position and low hole effective mass [13]. However,

*kinmanyu@cityu.edu.hk

RS-ZnO is a metastable phase and its synthesis is achieved only at high pressure (∼9 GPa) [14,15]. To facilitate the growth of RS-ZnO, one can alloy ZnO with a RS oxide (e.g., CdO, MgO, NiO) and/or grow it on a substrate with RS structure (e.g., MgO) [16–18]. Since NiO is a well-known wide-gap ($E_g \sim 3.8$ eV) p-type semiconductor with RS structure and an unusually high location of the VBE (i.e., approximately 4.8 eV below the vacuum level) [19], alloying of ZnO with RS-NiO would be of particular interest to achieve p-type dopable RS-ZnO-based alloys. A few earlier investigations have reported the synthesis and optoelectronic properties of ZnO-NiO alloys [18,20–23]. For instance, Katayama *et al*. grew RS-$Zn_{1-x}Ni_xO$ ($x > 9\%$) thin films on MgO (100) single-crystal substrates using pulsed-laser deposition [18], while Langell *et al*. synthesized RS-$Zn_{1-x}Ni_xO$ ($x > 0.68$) through a solid-state reaction [23]. Nevertheless, detailed investigations into the electronic band structure, phase stability, doping, and optoelectronic properties of RS-$Zn_{1-x}Ni_xO$ alloy thin films over a wide alloy composition range are still lacking.

Here, we report on the synthesis of transparent $Zn_{1-x}Ni_xO$ alloy thin films over the entire composition range by RF magnetron cosputtering with ZnO and NiO sputtering targets. We find that, as the Ni content increases, the $Zn_{1-x}Ni_xO$ alloy thin films undergo a WZ to RS structural phase transition with a large upward shift of the VBE by about 1 eV. RS-$Zn_{1-x}Ni_xO$ alloy thin films can exhibit p-type conductivity at room temperature by controlling cation vacancy and/or oxygen interstitial native defects via growth in an oxygen-rich environment. The p-type doping in RS-$Zn_{1-x}Ni_xO$ can also be realized by extrinsic doping with Cu. The optoelectronic and carrier transport properties are investigated in detail through a variety of analytical techniques.

II. EXPERIMENT

$Zn_{1-x}Ni_xO$ alloy thin films are grown on glass substrate using a multigun radiofrequency magnetron sputtering system with separate ZnO and NiO targets at an elevated substrate temperature of about 270 °C. The oxygen flow ratio, $f\,(O_2)/[f\,(Ar) + f\,(O_2)]$, in the sputtering gas is fixed at 0% (pure Ar) or 1.4%. Hereafter, for the convenience of discussion, we refer to films deposited in pure Ar and Ar^+ 1.4% O_2 as stoichiometric and O-rich films, respectively, although the determination of the exact stoichiometry of the films is difficult. The Cu doping (≤2%) is achieved by cosputtering with a metal Cu target. Alloy composition is controlled by varying the sputtering power of the individual targets. The composition and thickness of alloy films are determined by means of Rutherford backscattering spectrometry (RBS) using a 3.04-MeV He^{2+} beam. The crystal structure is analyzed by grazing-incidence x-ray diffraction (GIXRD) with a grazing incidence angle of 1°. Standard (isotropic) spectroscopic ellipsometry (SE) measurements are performed at room temperature in the photon energy range of 0.74–6.45 eV at incidence angles of $\Phi = 55$, 65, and 75° using a rotating-compensator instrument (J. A. Woollam, M-2000). Electrical properties are investigated by means of variable-temperature (300–450 K) Hall-effect measurements in the van der Pauw configuration using an Ecopia HMS-5500 system, while the room-temperature Seebeck measurements are conducted to verify the p- or n-type conductivity of the films with an MMR SB1000 system. High-resolution XPS measurements are performed using a monochromatic AlK x-ray source ($h\nu = 1.487$ keV). Photoelectrons are collected and analyzed with a concentric hemispherical analyzer. Positions of the VBM are measurement by means of ultraviolet ambient-pressure photoemission spectroscopy (UV-APS) with a KP Technology APS04 system using UV light excitation in the photon energy range of 3.4 –7 eV.

III. RESULTS AND DISCUSSION

A. Crystal structure

All as-sputtered $Zn_{1-x}Ni_xO$ thin films are polycrystalline with thicknesses in the range of 90–150 nm. Figure 1(a) shows the GIXRD spectra from a series of typical $Zn_{1-x}Ni_xO$ alloy thin films, with x ranging from zero to one. The grain size of these films is about 15 nm from the diffraction peak width using the Scherrer equation. As observed, the (002) diffraction peak is most prominent for WZ-ZnO. As NiO is alloyed with ZnO, the intensity of the (002) peak drops, while the intensity of the WZ phase (103) diffraction peak increases. It should be noted that the intensity of the (002) peak is largely reduced in the GIXRD measurement of thin films, with preferential orientation perpendicular to the substrate, since the scattering vector cannot be aligned with the surface normal. From the symmetric $\theta/2\theta$ XRD measurements (not shown), we find that the preferred orientation of these WZ-$Zn_{1-x}Ni_xO$ alloy thin films is along the c axis (001), with the strongest diffraction peak at (002). As the Ni content increases to $x \geq 0.27$, the GIXRD pattern changes, showing a strong peak at $2\theta \sim 36°$, which corresponds to the (111) diffraction peak from alloys with a RS structure. This RS-$Zn_{1-x}Ni_xO$ (111) diffraction peak shows a slight shift toward higher angle with increasing x, suggesting that the lattice parameter decreases. It is worth noting that the composition at which the phase transition occurs critically depends on the growth conditions (e.g., growth method, substrate, temperature, sputtering gas composition). For instance, Katayama *et al*. reported that epitaxial RS-$Zn_{1-x}Ni_xO$ was formed at a low level of Ni ($x = 0.09$) using pulsed-laser deposition on a MgO (100) substrate [18], while in our previous work we found that pure WZ-$Zn_{1-x}Cd_xO$ alloy thin films could be stable up to a much

higher Cd composition of $x \sim 0.72$, with a narrow mixed-phase region, when grown in an O-rich environment [16]. Here work, we find that the phase transition point can be slightly affected by the sputtering gas composition. Specifically, the lowest Ni content, x (i.e., $x = 0.27$), for a pure RS-$Zn_{1-x}Ni_xO$ alloy thin film is obtained when sputtered in a gas with 1.4% O_2, while the WZ phase is more stable for thin films with $x \leq 0.3$ when sputtered in pure Ar.

As shown in Fig. 1(b), the lattice parameter of the RS-$Zn_{1-x}Ni_xO$ alloy thin film reduces linearly as the Ni content x increases, in agreement with other reports in the literature [23,24]. By extrapolation, the lattice constant of RS-ZnO is about 4.41 Å, which is close to the experimental value of 4.28 Å estimated from high-pressure diffraction measurements [25]. Similarly, the lattice parameter of the WZ-$Zn_{1-x}Ni_xO$ alloy exhibits a reduction with increasing Ni content x (not shown). In the $Zn_{1-x}Ni_xO$ alloys, Ni is mainly located at the substitute site of Zn in the corresponding structure phase. Changes in the lattice parameter with composition can be understood by taking into account the ionic radii of Zn^{2+} and Ni^{2+} in the corresponding crystal structures with certain coordination number (Z). For the WZ phase structure, the radii of Zn^{2+} ($Z = 4$) and Ni^{2+} ($Z = 4$) are about 0.6 and 0.55 Å, respectively, while, in the RS phase structure, the radii of Zn^{2+} ($Z = 6$) and Ni^{2+} ($Z = 6$) are about 0.74 and 0.69 Å, respectively [26]. In both structures, the radius of Ni^{2+} is smaller than that of Zn^{2+}, leading to a reduction of the lattice parameter with increasing Ni content x.

B. Optical properties

The optical properties of $Zn_{1-x}Ni_xO$ alloy thin films are studied using SE. SE measures the relative change of the polarization state of light reflected (r_p and r_s) from (or transmitted through) the surface of a sample, providing unique advantages over the traditional transmittance-reflectance measurements. In reflection mode, SE yields the complex ratio, ρ, between the Fresnel reflection coefficients for p and s polarizations, i.e., $\rho \equiv r_p/r_s \equiv \tan\Psi \exp(i\Delta)$, where Ψ and Δ are the amplitude ratio and phase difference, respectively. In principle, the dielectric function, ϵ, of optically anisotropic materials, such as ZnO or ZnO alloys with WZ structures, can be expressed by the ordinary ($\bar{\varepsilon}_{\parallel}$) and extraordinary ($\bar{\varepsilon}_{\perp}$) components, corresponding to the electric field polarization perpendicular ($\mathbf{E} \perp \mathbf{c}$) and parallel ($\mathbf{E} \parallel \mathbf{c}$) to the optical axis, respectively [27–29]. Nevertheless, it is demonstrated that ϵ of ZnO from the isotropic fit yields ϵ similar to that of the ordinary $\bar{\varepsilon}_{\parallel}$ [30], and the extraordinary $\bar{\varepsilon}_{\perp}$ has a minor influence on (Ψ, Δ), far above the absorption edge [31]. Thus, the isotropic fit is a sufficient approach for an ellipsometry study of the WZ-structured ZnO- or ZnO-based alloys [29,32], which is also adopted in this work.

SE data analysis is based on the three-layer optical model, i.e., the glass substrate, $Zn_{1-x}Ni_xO$ film, and a surface roughness layer. For WZ-$Zn_{1-x}Ni_xO$ thin films, Psemi-M0 & Gaussian oscillators are used to describe their dielectric function, while only Gaussian oscillators are adopted for RS-$Zn_{1-x}Ni_xO$ alloys. These dielectric function models can fit the experimental SE data (Ψ, Δ) very well over the whole spectral range. Figure 2 shows the SE spectra (both measured and fitted values with an angle of incidence of 75°) for a typical WZ-$Zn_{0.85}Ni_{0.15}O$ alloy thin film, with a mean square error (MSE) around 2.23. Based on SE analysis, the dielectric function, i.e., $\varepsilon(E) = \varepsilon_1(E) + i\varepsilon_2(E)$, can be derived, where $\varepsilon_1(E)$ and $\varepsilon_2(E)$ are Kramers-Kronig transforms of each other. Figure 3(a) presents ε_1 of $Zn_{1-x}Ni_xO$ alloy thin films sputtered in pure Ar. It is worth noting that the obtained values of ϵ (including ε_1 and ε_2) of NiO and ZnO are comparable to values reported in the literature [28,33]. As shown in the ε_1 spectra, the free-exciton transition (from the uppermost VB with Γ_9 symmetry to the conduction band (CB) with Γ_7 symmetry [34,35], also referred to as A exciton) at a photon energy of about 3.3 eV is distinct at room temperature for the WZ-ZnO thin film. This peak is considerably broadened as x increases, resulting from alloying effects. Such an

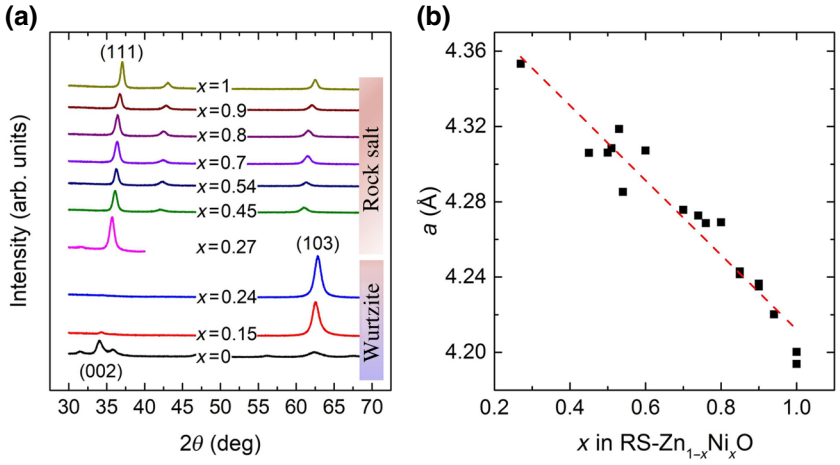

FIG. 1. (a) GIXRD spectra of $Zn_{1-x}Ni_xO$ alloy thin films with different Ni content x; (b) the lattice parameter of RS-$Zn_{1-x}Ni_xO$ alloy as function of x, with the red dashed line as the corresponding linear fit.

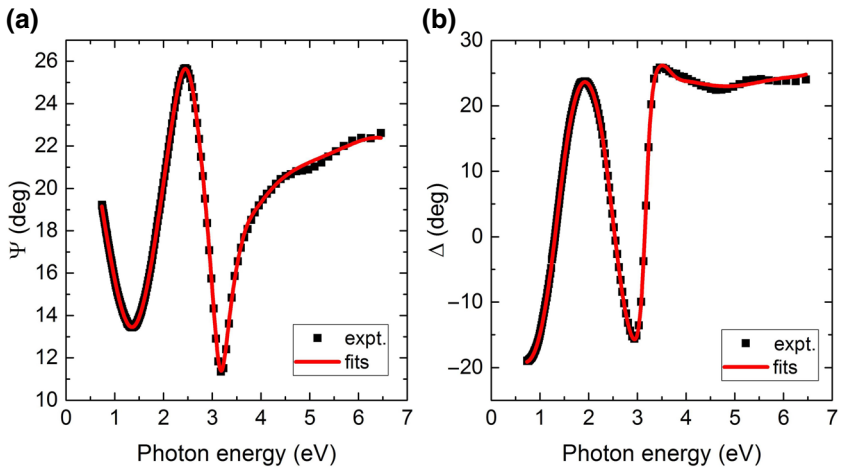

FIG. 2. Measured (black squares) and fitted (red solid lines) SE spectra [Ψ and Δ in (a),(b), respectively] of a $Zn_{0.85}Ni_{0.15}O$ thin film, with angle of incidence of 75°.

excitonic optical transition is also discernable from the ε_2 spectra (not shown) or optical absorption coefficient α. In contrast, the exciton peak in WZ-$Zn_{1-x}Mg_xO$ ($x < 0.21$) alloys does not show such distinct broadening as the Mg content increases, owing to its high exciton binding energy (approximately 60 meV), which apparently compensates for the alloy broadening effect [29,32,36]. Hence, it is very likely that the exciton binding energy for WZ-$Zn_{1-x}Ni_xO$ is much lower than that of WZ-ZnO or WZ-$Zn_{1-x}Mg_xO$. In addition, the exciton absorption energy of WZ-$Zn_{1-x}Ni_xO$ alloy film exhibits a blueshift with increasing x, which is similar to that of WZ-$Zn_{1-x}Mg_xO$ alloy thin films [27]. Figure 3(a) also reveals that, as the alloy undergoes the WZ-RS phase transition at $x \sim 0.27$, there is an abrupt change in the dielectric functions. This is understandable, since the dielectric function is determined by the band structure and the many-particle interaction of a given material [29,37]. For the RS-$Zn_{1-x}Ni_xO$ alloys, the main critical point at around 4 eV shows a redshift as x increases.

The complex refractive index $\tilde{n} = n + i\kappa$ can also be obtained from the dielectric function through the Maxwell relation, where n and κ are the refractive index and extinction coefficient, respectively. Figure 3(b) shows that n at $E = 2$ eV for the $Zn_{1-x}Ni_xO$ alloy thin films sputtered in pure Ar increases linearly with Ni content x for both the WZ and RS alloys. Notably, values of n for the RS structure alloys (∼2.2–2.4) are also significantly higher than those for the WZ alloys (approximately 2). The optical absorption coefficient α can be expressed in terms of the extinction coefficient as $\alpha = 4\pi\kappa/\lambda$. The values of α of $Zn_{1-x}Ni_xO$ alloy thin films with different x shown in Fig. 3(c) reveal that, with the addition of Ni to ZnO, the subgap absorption increases substantially. This is very similar to NiO or NiO-based alloys (e.g., $Ni_xCd_{1-x}O$), which is attributed to native defects, in particular, V_{Ni} which induces p-d charge-transfer transitions and/or to the d-d crystal-field transitions [38–40]. Hence, it is expected that the optical properties are strongly affected by varying the concentration of these native defects in these alloys. Since the formation of these cation vacancies becomes favorable under an O-rich environment [41], the concentration of these defects can be controlled by sputtering with a mixture of Ar and O_2. For comparison, we note that such high subgap absorption is not present in the WZ-$Zn_{1-x}Cd_xO$ alloy thin films over a wide composition range ($0 \le x \le 0.66$) [16]. Figure 3(d) compares the absorption coefficient spectrum of an O-rich $Zn_{0.49}Ni_{0.51}O$ film and that of a stoichiometric film with comparable composition ($Zn_{0.47}Ni_{0.53}O$). Notably the value of α in the subgap region (<4 eV) for the O-rich film with a higher concentration of V_{Ni} (and possibly O_i as well) is about five times higher than that of the stoichiometric alloy film. Hence, the magnitude of the subgap α value of RS-$Zn_{1-x}Ni_xO$ qualitatively describes the concentration of native acceptors (i.e., V_{Ni}, O_i), which, in turn, affects their p-type conductivity. This is discussed in Sec. C.

The optical band gaps (E_g^{opt}) are estimated in two different ways, i.e., (i) by a normal procedure of extrapolating α^2 versus photon energy plots to the energy intercept, and (ii) by using the second derivative of ϵ_1 (i.e., $d^2\varepsilon_1/dE^2$) [42,43]. For example, Fig. 4(a) shows $d^2\varepsilon_1/dE^2$ of the $Zn_{0.24}Ni_{0.76}O$ alloy; the black arrow indicates the band-gap energy. Since the $Zn_{1-x}Ni_xO$ alloy thin films are semi-insulating or with a low carrier density (i.e., $<10^{19}$ cm^{-3}), free carrier effects (i.e., the Burstein-Moss shift effect and the band-gap-renormalization effect) on the band-gap measurements are negligible [44], and the measured E_g^{opt} values correspond to the intrinsic band gap (E_g). Figure 4(b) shows values of E_g of $Zn_{1-x}Ni_xO$ alloys with different x obtained by both methods. In general, E_g values estimated from α^2 extrapolation are much lower than those derived from $d^2\varepsilon_1/dE^2$, especially for RS-$Zn_{1-x}Ni_xO$ alloys. For the RS-$Zn_{1-x}Ni_xO$ alloys, the E_g decreases as x increases, which is also evidenced from the redshift of the main critical point in ε_1. While for the WZ-$Zn_{1-x}Ni_xO$ alloy thin films, the E_g values extracted from α^2 and $d^2\varepsilon_1/dE^2$ exhibit opposite trends, i.e., the former and latter show a decrease and an increase with x, respectively. As is well

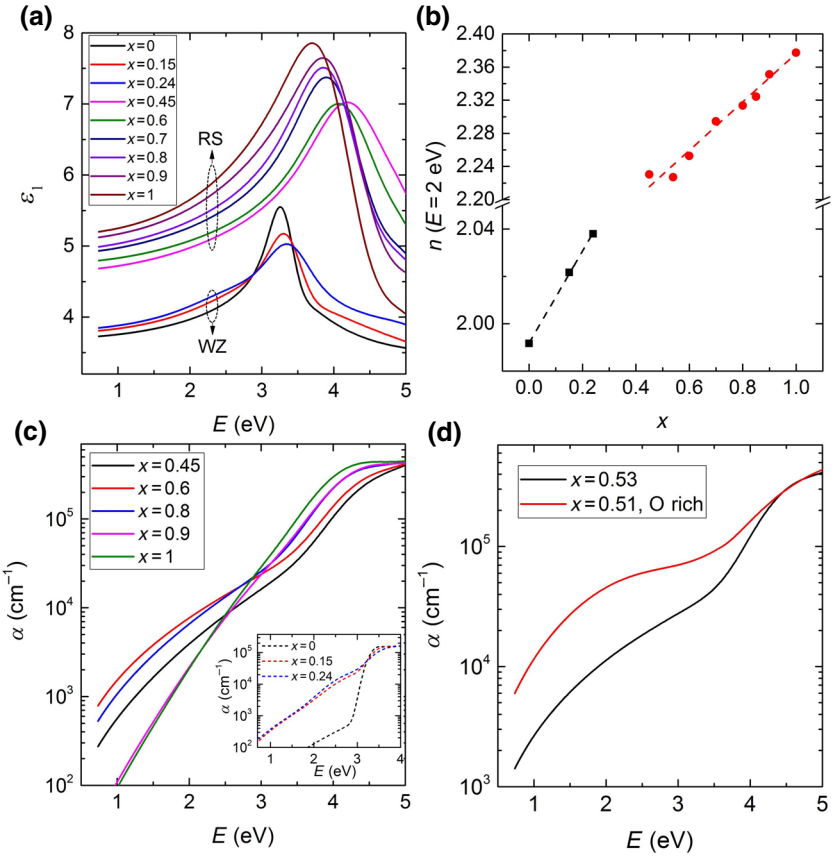

FIG. 3. (a) Real part (ϵ_1) of the dielectric function, (b) refractive index n at $E = 2$ eV, and (c) optical absorption coefficient α for RS-$Zn_{1-x}Ni_xO$ thin films with different Ni content x (sputtered in pure Ar); the inset of (c) shows α for the WZ-$Zn_{1-x}Ni_xO$ thin films. (d) Values of α of RS-$Zn_{0.47}Ni_{0.53}O$ and $Zn_{0.49}Ni_{0.51}O$ sputtered in pure Ar and Ar with 1.4% O_2, respectively.

known, the band edge of semiconductor alloys is typically broadened due to localized states, and such broadening would cause an uncertainty in determining the band gap using the Tauc method [45,46]. Moreover, using the Tauc method, the obtained band-gap value relies critically on values taken for straight-line extrapolation. To alleviate such uncertainties, band-gap determination for these alloy semiconductors based on the derivative method is preferred [45]. The E_g values of WZ-ZnO and RS-NiO derived from $d^2\varepsilon_1/dE^2$ are 3.25 and 3.83 eV, respectively, which are in agreement with values reported in the literature. Thus, the E_g values derived from the $d^2\varepsilon_1/dE^2$ method are used in this work, unless otherwise specified.

The deviation of E_g of a semiconductor alloy, A_xB_{1-x}, from the Vegard law is usually described by using a bowing parameter, b, $E_g(x) = xE_A + (1-x)E_B - bx(1-x)$, with E_A and E_B as the band gap of two-end materials A and B, respectively. Fitting the band-gap data of RS-$Zn_{1-x}Ni_xO$ alloys obtained by the Tauc and derivative methods using the bowing equation results in bowing parameters $b = 0.6$ and 1.0 eV, respectively. The fitted curves are also shown as the black and red dashed lines in Fig. 4(b). RS-ZnO is an indirect gap semiconductor with an E_g value of about 2.45 eV (L-Γ and Σ-Γ), while the strong direct optical transition occurs at about 4.5 eV [47]. Using the bowing parameter from the derivative method, the E_g value of RS-ZnO can be estimated to be 5.0 eV. It is worth noting that the 4.5 eV direct transition for RS-ZnO reported in Ref. [47] is obtained under high pressure and using α^2 extrapolation, and hence, may suffer from the uncertainties discussed above. Furthermore, we note that the indirect band gap for RS-ZnO cannot be reliably determined, since the absorption coefficient for an indirect transition ($<10^3$ cm^{-1} [48,49], e.g., α of intrinsic silicon at the indirect band-gap energy is <10 cm^{-1}) is orders of magnitude lower than that of the direct one [18,37,50,51]. Although no experimental results on the band gap of WZ-NiO have been reported, by extrapolating the limited number of band-gap data points of WZ-$Zn_{1-x}Ni_xO$, we can also estimate that the band gap for WZ-NiO is about 4 eV.

C. Electrical transport mechanism

The electrical properties of semiconducting ZnO-NiO alloy thin films are investigated by variable-temperature Hall-effect measurements in the temperature range of 300–450 K. We find that stoichiometric alloy films are semi-insulating and only exhibit low conductivity ($<10^{-2}$ S/cm) at high temperature ($T \geq 400$ K). On the other hand, O-rich and/or Cu-doped RS-$Zn_{1-x}Ni_xO$ alloys exhibit measurable conductivity at temperatures close to room temperature (i.e., $300 \leq T \leq 350$ K). Interestingly, all conducting RS-$Zn_{1-x}Ni_xO$ alloy thin films show p-type conductivity in the measurement temperature range.

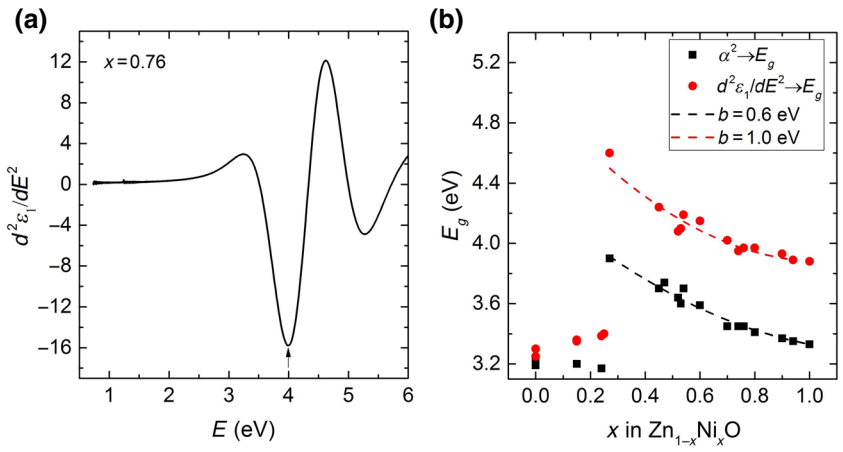

FIG. 4. (a) $d^2\varepsilon_1/dE^2$ of $Zn_{0.24}Ni_{0.76}O$ alloy as function of photon energy; the black arrow indicates the direct band-gap energy. (b) E_g of $Zn_{1-x}Ni_xO$ alloy thin films with different x; the black squares and red circles indicate the values derived from α^2 and $d^2\varepsilon_1/dE^2$, respectively.

Similar to NiO or NiO-based alloy semiconductors (e.g., O-rich $Ni_xCd_{1-x}O$) [40,52], the hole mobility (μ_h) for these p-type RS-$Zn_{1-x}Ni_xO$ alloy thin films is very low (<0.1 cm^2/Vs) at close to room temperature (<350 K). Consequently, although the resistivity, ρ, can be measured for these O-rich alloys at room temperature, the conductivity type determined from the Hall-effect measurement using a typical magnetic field of 0.5 T is not reliable. Hence, room-temperature Seebeck measurements are also performed on these samples to confirm their conductivity type. The measured Seebeck coefficients (S) for all O-rich RS-$Zn_{1-x}Ni_xO$ alloys are positive, and thus, confirm the p-type conductivity of these alloys. Moreover, S also shows a monotonous decrease with increasing Ni content x. For example, the values of S for the O-rich RS alloys with $x = 0.27$, 0.51, and 0.82 are 130, 109, and 55 μV/K, respectively. It should be noted that the value of S of a semiconductor is related to its carrier density, and its magnitude decreases with increasing carrier concentration [52,53]. Hence, our results suggest that the hole concentration in these alloys increases with the Ni content x.

As mentioned above, μ_h is too small to be reliably measured from the room-temperature Hall-effect measurements for these RS-$Zn_{1-x}Ni_xO$ alloy thin films. However, we observe that, similar to our earlier report on O-rich CdNiO alloys [40], μ_h increases with measurement temperature and, at >380 K, Hall measurements on the carrier concentration and mobility become reliable due to a higher mobility of $\mu_h > 1$. The hole concentration (N) and μ_h for RS-$Zn_{1-x}Ni_xO$ alloy thin films, with different x at relatively high temperature, ranging from 380 to 450 K, are shown in Figs. 5(a) and 5(b), respectively. As seen in Fig. 5(a), the hole concentration, N, does not significantly change with temperature. Hence, we can reasonably assume that hole concentration N (room temperature) = N (380 K) and estimate the room-temperature μ_h from the room-temperature resistivity, ρ. For example, the estimated room-temperature μ_h values for O-rich RS-$Zn_{0.19}Ni_{0.82}O$ and $Zn_{0.49}Ni_{0.51}O$ are about 0.35 and 0.49 cm^2/Vs, respectively. Nevertheless, these room-temperature μ_h values are very likely overestimated, especially for alloys with high x, the N of which exhibits a slight reduction in the high-temperature regime, as seen in Fig. 5(a). Similar to O-rich NiO [40,54], this can be attributed to the thermal instability of O-induced V_{Ni} or O_i in these alloy thin films. We also note that, for the O-rich RS alloys, N increases with increasing Ni content x, in good agreement with the Seebeck coefficient measurements. In comparison with the undoped samples, O-rich Cu-doped (approximately 2%) alloy with similar composition ($x \sim 0.5$) shows about three times higher hole concentration and lower resistivity. For stoichiometric alloys, in contrast to the undoped alloy with $x \sim 0.76$, Cu-doped RS-$Zn_{0.26}Ni_{0.74}O$ exhibits p-type conductivity at slightly higher above room temperature (320 K) and does not show a significant reduction in hole concentration as the temperature increases, which implies that the p-type conductivity arises from Cu acceptors and they are thermally more stable than native acceptor defects. Although this stoichiometric Cu-doped $Zn_{0.26}Ni_{0.74}O$ sample is too resistive to measure at room temperature [see Figs. 5(c) or 5(d)], we estimate its room-temperature resistivity by extrapolating the linear fit of $\ln(\rho/T)$, as given in Fig. 5(d), to be about 3700 Ω cm, with a calculated room-temperature hole mobility of about 0.08 cm^2/Vs, which is close to the μ_h (i.e., 0.07 cm^2/Vs) of O-rich NiO from previous reports [40,55]. The Kroger-Vink notation [56] can be used to describe the hole-generation mechanism in these p-type RS-ZnNiO alloy thin films due to native defects and Cu dopants. For the p-type O-rich ZnNiO thin films, analogous to O-rich NiO, the primary native acceptor defect (i.e., V_{Ni} and/or O_i) formation reactions can be written as

$$\frac{1}{2}(O_2)_g \rightleftharpoons O_o + V_{Ni}, \quad (1)$$

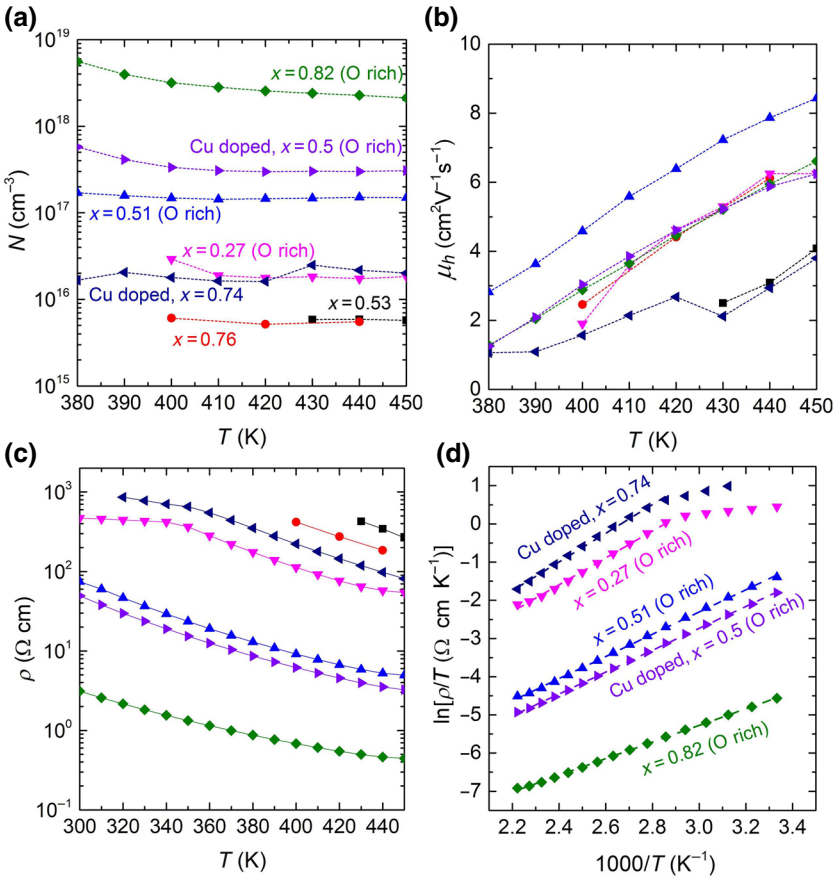

FIG. 5. Temperature-dependent electrical properties from Hall-effect measurements for p-type RS-$Zn_{1-x}Ni_xO$ alloy thin films in the temperature range of 300–450 K, (a) the hole concentration, N; (b) hole mobility, μ_h; (c) resistivity, ρ; and (d) plots of $\ln(\rho/T)$ versus $1/T$, as well as the corresponding linear fits (dotted lines).

and

$$\frac{1}{2}(O_2)_g \rightleftharpoons O_i. \tag{2}$$

While V_{Ni} and O_i can generate singly or doubly ionized vacancies with free holes, according to the following reactions:

$$V_{Ni} \rightleftharpoons V'_{Ni} + \oplus\,, \tag{3}$$
$$V'_{Ni} \rightleftharpoons V''_{Ni} + \oplus, \tag{4}$$
$$O_i \rightleftharpoons O'_i + \oplus, \tag{5}$$
$$O'_i \rightleftharpoons O''_i + \oplus. \tag{6}$$

For Cu-doped samples, Cu (with a valence state of Cu^+) substitutes Zn or Ni, forming Cu_{Zn} and/or Cu_{Ni} that can also give rise to free holes, according to following reactions:

$$Cu_{Zn} \rightleftharpoons Cu'_{Zn} + \oplus, \tag{7}$$

$$Cu_{Ni} \rightleftharpoons Cu'_{Ni} + \oplus. \tag{8}$$

The temperature-dependent μ_h values for various RS alloy samples in the temperature range of 380–450 K shown in Fig. 5(b) reveal that μ_h generally increases with temperature. This also suggests that the conduction process in these p-type RS-$Zn_{1-x}Ni_xO$ alloy thin films is possibly due to the thermal excitation of mobility, i.e., small polaron hopping (SPH), as observed in NiO and O-rich $Ni_xCd_{1-x}O$ alloys [40,52,57]. Figure 5(c) gives the corresponding resistivity in the temperature range of 300–450 K. As expected, the resistivity decreases with temperature, which is a typical characteristic of a semiconductor. Based on the SPH model, the temperature-dependent resistivity can be expressed as $\rho/T = \rho_0 \exp(E_a/kT)$, where k is the Boltzmann constant and E_a is the activation energy [58]. Figure 5(d) shows the $ln(\rho/T)$ versus $1/T$ plots and their corresponding fits for the RS-$ZnO_{1-x}Ni_xO$ alloy thin films with relatively low ρ. As obtained, data fit well with the SPH model in the temperature range 300–450 K. E_a extracted from the slopes of the fits varies from 0.19 (O-rich $Zn_{0.18}Ni_{0.82}O$) to 0.32 eV (Cu-doped $Zn_{0.26}Ni_{0.74}O$); the E_a value of O-rich $Zn_{0.18}Ni_{0.82}O$ is close to that of room-temperature-sputtered O-rich NiO (i.e., 0.17 eV) [40]. We note that the O-rich $Zn_{0.18}Ni_{0.82}O$ sample with much poorer crystallinity has a smaller E_a. The reduced E_a would likely result from structural disorder, which introduces a broad distribution of native acceptor states (e.g., V_{Ni}) above the VB [59]. Obviously, E_a is also related to the Ni content x, since the concentration of V_{Ni} would

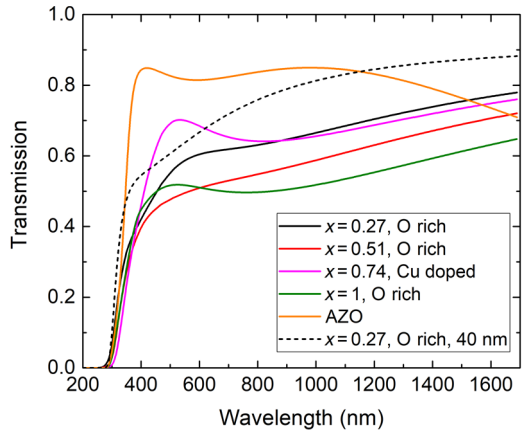

FIG. 6. Transmission spectra of typical RS-$Zn_{1-x}Ni_xO$ alloy thin films (100 nm on glass substrate) with p-type conductivity. Transmission spectra of O-rich NiO and AZO thin films are also included for comparison. Dashed line represents the transmission of O-rich $Zn_{0.73}Ni_{0.27}O$ film with thickness of 40 nm.

be proportional to Ni sites available in the thin film. In addition to the native acceptor defects, the p-type conductivity of RS-$Zn_{1-x}Ni_xO$ alloys can be further improved by optimizing the Cu dopant concentration. For extrinsic doping, Li would also be an ideal p-type dopant for NiO-based alloys [60], which will be investigated in our future work. To further reveal the transparency of these p-type ZnNiO alloy thin films, Fig. 6 compares the transmission of p-type ZnNiO films with p-type O-rich NiO and a conventional n-type transparent conducting oxide [Al-doped ZnO(AZO)]. All transmission spectra shown in Fig. 6 are for thin films of 100 nm on glass substrates. As observed, the O-rich RS-$Zn_{1-x}Ni_xO$ alloy with relatively low x (e.g., $x = 0.27$) and the Cu-doped RS-$Zn_{1-x}Ni_xO$ alloy (e.g., $x = 0.74$) exhibit relatively high transmission (approximately 70%), slightly lower than that of n-type AZO thin film. The O-rich RS-$Zn_{1-x}Ni_xO$ alloy with high x (e.g., $x = 0.82$) shows relatively low transmission (approximately 50%). As mentioned earlier, the low transmittance of O-rich RS-$Zn_{1-x}Ni_xO$ alloy with high Ni content x can be attributed to absorption due to a high concentration of native defects (e.g., V_{Ni}). Notably, for applications as hole-transport layers or p-type emitters in devices, only 10–40 nm film thickness is required (for comparison, the transmission of O-rich $Zn_{0.73}Ni_{0.27}O$ with a thickness of 40 nm is also given in Fig. 6, as shown by the dashed line). Hence, the transmittance of these p-type layers can be >80%, which makes p-type RS-$Zn_{1-x}Ni_xO$ suitable for transparent electronic devices.

D. Electronic band structure

The electronic band structure of these $Zn_{1-x}Ni_xO$ alloy thin films are further studied by means of XPS and UV-APS. High-resolution core-level XPS spectra of Zn 2p, O 1s, and Ni 2p are recorded for the alloy thin films with different x and/or Cu doping. We find that the O stoichiometry or Cu doping do not have a noticeable effect on the core-level XPS spectra. Thus, only XPS spectra for stoichiometric thin films with representative Ni content x are shown in Fig. 6 (except $x = 0.27$, which is O rich). All spectra are recorded after brief Ar^+ sputtering to remove surface contamination. The binding energies (E_b) are referenced to the C 1s peak (collected without Ar^+ sputtering) at 284.8 eV. The measured Zn $2p_{3/2}$ peak position for WZ-ZnO in this work is comparable to values reported by others [61]. Figure 7(a) shows that E_b for the Zn $2p_{3/2}$ core-level peak is not sensitive to the Ni content and no significant shift is observed. O 1s spectra for $Zn_{1-x}Ni_xO$ alloys for different x shown in Fig. 7(b) can be resolved into two different components, i.e., a main peak at lower E_b and a weaker side peak at high E_b. The main O 1s peak for the two end materials (i.e., WZ-ZnO and RS-NiO) are consistent with reported values for Zn − O and Ni − O bonds [61,62], while the side peak at higher E_b can be ascribed to O in a different bonding environment (e.g., O interstitials; Ni vacancies; or surface-adsorbed OH, COOH, and Ni_2O_3 groups) [63]. Notably, the E_b value of the main O 1s peak for WZ-ZnO is slightly lower than that of the RS-NiO phase by about 0.2 eV. The E_b has a small increase with x in the WZ phase. However, a strong shift to lower binding energy is observed at the WZ to RS phase transition, so that the O 1s peak for RS-$Zn_{0.73}Ni_{0.27}O$ is shifted to a lower energy by about 0.5 eV. As x increases, this peak gradually shifts back to the E_b value for RS-NiO. The concentration of defect-related O in the film would affect the hole N, such that O_i or V_{Ni} are believed to be effective acceptor defects in NiO and its alloys. Since the E_b value of this peak is much higher than that of the main peak, it is consistent with V_{Ni} acceptors with Ni^{3+} valency in Ni_3O_2. Nevertheless, a quantitative correlation between this high E_b peak with hole N cannot be established.

Figure 7(c) shows the Ni $2p_{3/2}$ spectra of $Zn_{1-x}Ni_xO$ alloy thin films with different x. The various features of the Ni $2p_{3/2}$ spectra are similar for all RS-$Zn_{1-x}Ni_xO$ alloy thin films, and they are labeled in Fig, 7(c) as A ($2p^5 3d^9 \underline{Z}$), B ($2p^5 3d^9 \underline{L}$), and C ($2p^5 3d^8$), corresponding to the Zhang–Rice doublet bound states near the Fermi level and a hole in the O 2p ligand states [64–66]. The intensity ratio of peaks B to A increases with increasing x, which indicates that the Ni 3d states are modified by the addition of Zn in the alloy. Such modification of Ni 3d states with alloy composition are also found in other NiO-based alloy systems (e.g., $Ni_xCd_{1-x}O$, $Mg_xNi_{1-x}O$) [40,65]. Peak D, with $E_b \sim 851.8$ eV, in the Ni $2p_{3/2}$ spectra can be attributed to the formation of metallic Ni clusters due to the Ar^+ sputtering process [66]. For the Cu-doped samples, the Cu 2p XPS results are also recorded [see Fig. 7(d)]. The Cu 2p XPS spectrum from the Cu-doped $Zn_{0.26}Ni_{0.74}O$ alloy thin film [Fig. 7(d)] shows a single $2p_{3/2}$ peak at

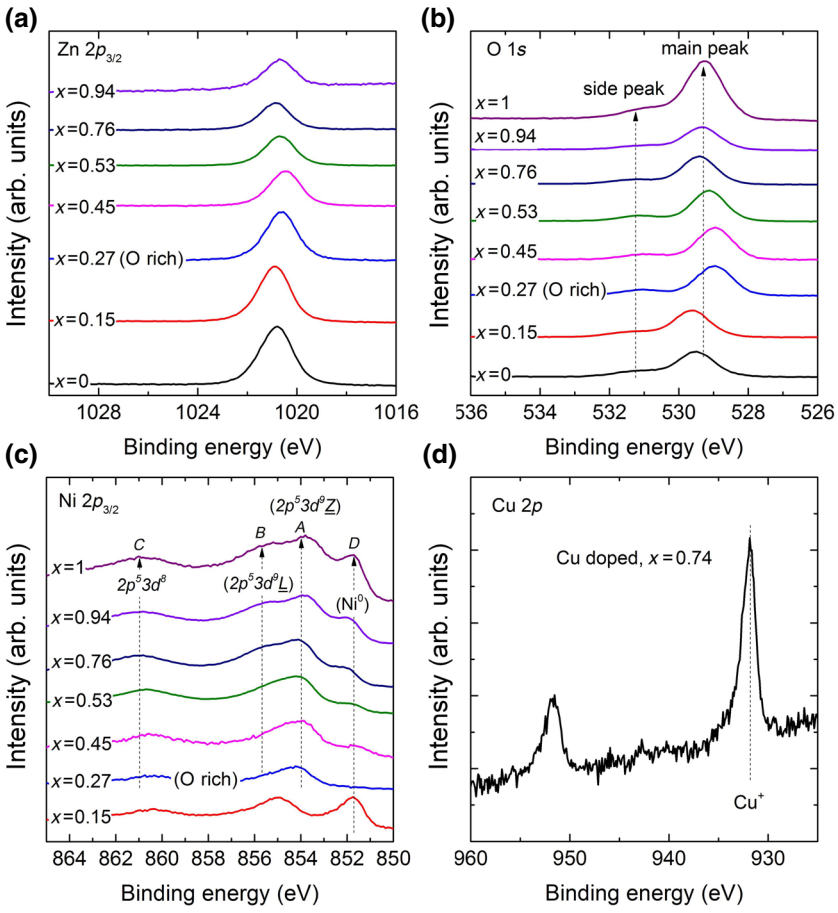

FIG. 7. High-resolution XPS core-level spectra of Zn $2p_{3/2}$ (a), O 1s (b), and Ni $2p_{3/2}$ (c) for $Zn_{1-x}Ni_xO$ alloy thin films with different Ni content x. (d) Cu $2p$ core-level spectrum for the Cu-doped $Zn_{0.26}Ni_{0.74}O$ alloy thin film.

$E_b \sim 931.9$ eV, which can be attributed to Cu^+. The possible presence of Cu^{2+} with $E_b \sim 934$ eV [67] is not observed in the spectrum, and hence, can be excluded. This indicates that the holes in these Cu-doped RS-$Zn_{1-x}Ni_xO$ samples have a contribution from Cu^+, similar to that of Cu-doped NiO [68].

The variation of the VBM of $Zn_{1-x}Ni_xO$ alloy thin films with alloy composition is studied by UV-APS and XPS valence band measurements. UV-APS measures the number of photoelectrons that are emitted from the sample illuminated by the tunable monochromatic UV light (3.4–7 eV). Photoelectrons can only be emitted from the sample if the photon energy is greater than that of E_F of a metal or VBM of a semiconductor. No photoelectrons are observed for the WZ-$Zn_{1-x}Ni_xO$ films. This suggests that the VBM, with respect to the vacuum-level E_{vac} of all WZ-$Zn_{1-x}Ni_xO$ alloys with x up to 0.24, is >7 eV. For the UV-APS measurement, the intensity of photoemission is normalized and processed by the cube root power law [69]. Figure 8(a) illustrates photocurrent data for the $Zn_{0.47}Ni_{0.53}O$ alloy film on a glass substrate; the VBM value (i.e., 5.48 eV below the vacuum level) is determined by extrapolating the linear part of the curve down to the baseline signal level. For comparison, the VBMs are also extracted from their XPS valence band spectra, i.e., by a linear extrapolation of the leading edge of the VB to zero baseline intensity. It is demonstrated that the Fermi level of semiconductors at the surface is pinned to a universal energy level, known as the Fermi-level stabilization energy, E_{FS}, located about 4.9 eV below the vacuum level, which is the Fermi level at which the formation energies of native donors and acceptors are equal [70]. Since XPS and APS are surface-sensitive techniques, the VBM measured can be referenced to E_{FS}. Absolute values of the VB maximum with respect to the E_{vac} of several oxide materials are determined using E_{FS} as the reference level [71,72]. Figure 8(b) compares values of the VBM for $Zn_{1-x}Ni_xO$ alloy thin films from UV-APS measurements (only for the RS phase) with those measured by XPS. The XPS results show that the VBM energy increases from −7 eV (for ZnO) to around −6.4 eV ($x = 0.24$) with increasing Ni content x for the WZ structure alloys. A drastic jump in the VBM energy is observed for the alloy with $x = 0.27$, when the alloy crystallizes in the RS structure. For the RS-$Zn_{1-x}Ni_xO$ alloys with $x \geq 0.27$, VBM energies obtained from the two approaches are comparable and increases slightly from about −5.5 to −5.0 eV (for NiO). The solid lines indicating the VBM (blue) and

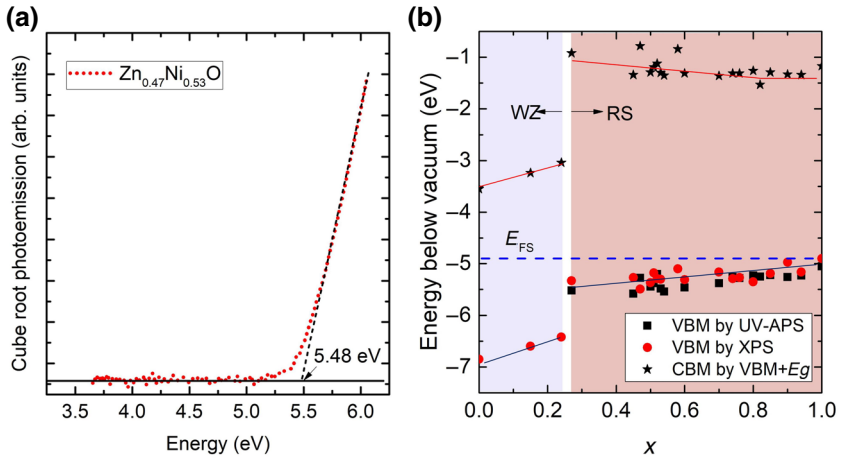

FIG. 8. (a) UV-APS data for the $Zn_{0.47}Ni_{0.53}O$ alloy film on a glass substrate, with VBM determined by extrapolating the linear part of the curve down to the baseline signal level. (b) VBM values extracted from two different measurements, i.e., UV-APS (black squares, only for RS phase) and XPS (red circles), for $Zn_{1-x}Ni_xO$ alloy thin films with varying Ni content x. The blue dotted line indicates the Fermi-level stabilization energy (E_{FS}). CBM energies calculated using the VB values and band-gap values from Fig. 4(b) are also shown (black stars).

CBM (red) are not best fits, but drawn only to guide the eye.

Figure 8(b) also shows the CBM obtained from the VBM values and the band gap obtained with the derivative method [Fig. 4(a)] for the $Zn_{1-x}Ni_xO$ alloys. Although the XPS results show that the VBM energy of the WZ alloys lies within the range of -6.5 to -7 eV, since the UV-APS measurements do not yield any photoelectron, we believe that XPS data are overestimating their VBM position. This may be because some of the photoelectrons collected are coming from regions deeper than the surface pinning layer in the XPS measurements. The UV-APS measurements, on the other hand, are much more surface sensitive. At the WZ to RS transition composition, we observe that the band structure of the two phases has a type II band alignment with the VBM of the RS phase >1 eV above that of the WZ phase. This is in excellent agreement with the band offset of WZ and RS ZnO calculated by hybrid density functional theory [13].

It is established that, when the CBM (VBM) of a semiconductor is close to E_{FS}, the Fermi energy level at which the formation energy of donor and acceptor defects are equal and is about -4.9 eV from E_{vac}, and thus, it is energetically favorable to form donor (acceptor) defects in the semiconductor. Hence, the drastic increase of the VBM by >1 eV as the alloys transform from the WZ to RS structure draws the VBM closer to E_{FS} and favors the formation of acceptor native (V_{Ni} and/or O_i) defects in the RS alloys. This is consistent with our observation that the RS alloys can exhibit p-type conductivity, especially when grown in an O-rich environment, where the formation of these native acceptor defects is more favorable. Moreover, due to the much higher location of the VBM for the RS alloys, ionization energies for extrinsic acceptors are expected to become much smaller, and hence, doping efficiency will be improved. This suggests that extrinsic doping with acceptors, such as Li, Cu, or Ag, can be further optimized to achieve high-conductivity p-type RS-ZnNiO alloys.

IV. CONCLUSIONS

Crystalline ZnO-NiO alloy thin films over the entire composition range are synthesized by radiofrequency magnetron sputtering on glass substrate at a substrate temperature of about 270 °C. We find that $Zn_{1-x}Ni_xO$ alloys are in the WZ structure for $x < 0.27$, while they become the RS structure as the Ni content increases to $x > 0.27$. The E_g of WZ-$Zn_{1-x}Ni_xO$ alloy thin films shows a slight increase with x, while the E_g of RS-$Zn_{1-x}Ni_xO$ alloys is about 4.6 eV at the WZ to RS transition composition and decrease with x to the value of RS-NiO (approximately 3.8 eV). Spectroscopic ellipsometry measurements show that the dielectric function of the RS alloys is significantly different from that of the WZ alloys. At 2 eV, the refractive index n is about 2 for the WZ alloys and about 2.2–2.4 for the RS alloys. Electrically, we find that nominally undoped stoichiometric $Zn_{1-x}Ni_xO$ alloys are semi-insulating at room temperature. However, p-type conductivity is observed in O-rich undoped and Cu-doped RS-$Zn_{1-x}Ni_xO$ alloy thin films. Variable-temperature Hall-effect measurements reveal that the hole mobility of O-rich RS-$Zn_{1-x}Ni_xO$ alloy thin film increases with temperature, which is consistent with hole transport via a SPH process with an activation of 0.19 ($x = 0.82$) to 0.32 eV ($x = 0.74$). Drastic differences in the electronic structure of the WZ and RS $Zn_{1-x}Ni_xO$ alloys are also observed with a type II band offset of the alloys at the WZ to RS transition composition. The VBM of the RS phase is >1 eV above that of the WZ phase, making them energetically favorable for the formation of native acceptor defects. The much higher VBM position of RS alloys also favors their extrinsic p-type doping efficiency.

ACKNOWLEDGMENTS

This work is supported by the General Research Fund of the Research Grants Council of Hong Kong SAR, China, under Projects No. CityU 11305119 and No. CityU-SRG

7005106, a start-up fund from Shantou University under Projects No. NTF18027 and No. NTF18021, the Major Research Plan of the National Natural Science Foundation of China (Project No. 91950101), and the Optics and Photoelectronics Project (Grant No. 2018KCXTD011). K.E. is supported by the Hong Kong Ph.D. Program (Grant No. PF16-02083), Research Grants Council, University Grants Committee, Hong Kong.

[1] S. C. Dixon, D. O. Scanlon, C. J. Carmalt, and I. P. Parkin, n-type doped transparent conducting binary oxides: An overview, J. Mater. Chem. C **4**, 6946 (2016).

[2] Z. Ye, H. He, and L. Jiang, An effective strategy for achieving stable p-type ZnO thin films, Nano Energy **52**, 527 (2018).

[3] C. Xie, X. T. Lu, X. W. Tong, Z. X. Zhang, F. X. Liang, L. Liang, L. B. Luo, and Y. C. Wu, Recent progress in solar-blind deep-ultraviolet photodetectors based on inorganic ultrawide bandgap semiconductors, Adv. Funct. Mater. **29**, 1806006 (2019).

[4] X. Xie, B. Li, Z. Zhang, and D. Shen, Reinventing a p-type doping process for stable ZnO light emitting devices, J. Phys. D: Appl. Phys. **51**, 225104 (2018).

[5] K. Tang, S.-L. Gu, J.-D. Ye, S.-M. Zhu, R. Zhang, and Y.-D. Zheng, Progress of the native defects and p-type doping of zinc oxide, Chinese Phys. B **26**, 047702 (2017).

[6] S. J. Pearton and F. Ren, p-type doping of ZnO films and growth of tenary ZnMgO and ZnCdO: Application to light emitting diodes and laser diodes, Int. Mater. Rev. **59**, 61 (2014).

[7] B. A. D. Williamson, J. Buckeridge, J. Brown, S. Ansbro, R. G. Palgrave, and D. O. Scanlon, Engineering valence band dispersion for high mobility p-type semiconductors, Chem. Mater. **29**, 2402 (2017).

[8] H. Kawazoe, H. Yanagi, K. Ueda, and H. Hosono, Transparent p-type conducting oxides: Design and fabrication of p-n heterojunctions, MRS Bull. **25**, 28 (2000).

[9] V. A. Ha, F. Ricci, G. M. Rignanese, and G. Hautier, Structural design principles for low hole effective mass s-orbital-based p-type oxides, J. Mater. Chem. C **5**, 5772 (2017).

[10] N. Sarmadian, R. Saniz, B. Partoens, and D. Lamoen, Easily doped p-type, low hole effective mass, transparent oxides, Sci. Rep. **6**, 20446 (2016).

[11] G. Hautier, A. Miglio, G. Ceder, G. M. Rignanese, and X. Gonze, Identification and design principles of low hole effective mass p-type transparent conducting oxides, Nat. Commun. **4**, 2292 (2013).

[12] M. Ting, K. M. Yu, M. Jaquez, I. D. Sharp, Y. Ye, N. Segercrantz, R. Greif, S. S. Mao, C. P. Liu, and W. Walukiewicz, $ZnO_{1-x}Te_x$ highly mismatched alloys beyond the dilute alloy limit: Synthesis and electronic band structure, J. Appl. Phys. **125**, 155702 (2019).

[13] A. Goyal and V. Stevanović, Metastable rocksalt ZnO is p-type dopable, Phys. Rev. Mater. **2**, 084603 (2018).

[14] F. Decremps, J. Pellicer-Porres, F. Datchi, J. P. Itié, A. Polian, F. Baudelet, and J. Z. Jiang, Trapping of cubic ZnO nanocrystallites at ambient conditions, Appl. Phys. Lett. **81**, 4820 (2003).

[15] S. Desgreniers, High-density phases of ZnO: Structural and compressive parameters, Phys. Rev. B **58**, 14102 (1998).

[16] C. Y. Ho, C. P. Liu, Y.-C. Chen, Z.-Q. Huang, F.-C. Chuang, and K. M. Yu, Effects of oxygen stoichiometry on the phase stability of sputter-deposited $Cd_xZn_{1-x}O$ alloys, Phys. Rev. Mater. **3**, 074605 (2019).

[17] C. Y. J. Lu, Y. T. Tu, T. Yan, A. Trampert, L. Chang, and K. H. Ploog, Growth and stability of rocksalt $Zn_{1-x}Mg_xO$ epilayers and ZnO/MgO superlattice on MgO (100) substrate by molecular beam epitaxy, J. Chem. Phys. **144**, 214707 (2016).

[18] S. Katayama, H. Hayashi, F. Oba, and I. Tanaka, Epitaxial growth and characterization of rocksalt ZnO thin films with low-level NiO alloying, Jpn. J. Appl. Phys. **50**, 075503 (2011).

[19] R. Deng, B. Yao, Y. F. Li, Y. M. Zhao, B. H. Li, C. X. Shan, Z. Z. Zhang, D. X. Zhao, J. Y. Zhang, D. Z. Shen, and X. W. Fan, X-Ray photoelectron spectroscopy measurement of n-ZnO/p-NiO heterostructure valence-band offset, Appl. Phys. Lett. **94**, 022108 (2009).

[20] J. Wang, X. Dong, B. Zhang, Y. Zhang, H. Wang, Z. Shi, S. Zhang, W. Yin, and G. Du, p-type NiZnO thin films grown by photo-assist metal-organic chemical vapor deposition, J. Alloys Compd. **579**, 160 (2013).

[21] M. Nishitani, M. Sakai, and Y. Monta, The wide band p-type material formed by the thin film with ZnO-NiO mixed crystal system, Mater. Res. Soc. Symp. Proc. **1538**, 399 (2013).

[22] Y. D. Zhao, X. Dong, Z. Z. Ma, Y. T. Zhang, B. Wu, S. W. Zhuang, B. L. Zhang, W. C. Li, and G. T. Du, High hole concentration Li-doped NiZnO thin films grown by photo-assisted metal–organic chemical vapor deposition, J. Cryst. Growth **454**, 30 (2016).

[23] K. J. Gaskell, A. Starace, and M. A. Langell, $Zn_xN_{1-x}O$ rocksalt oxide surfaces: Novel environment for Zn^{2+} and its effect on the NiO band structure, J. Phys. Chem. C **111**, 13912 (2007).

[24] S. D. Singh, V. Nandanwar, H. Srivastava, A. K. Yadav, A. Bhakar, P. R. Sagdeo, A. K. Sinha, and T. Ganguli, Determination of the optical gap bowing parameter for ternary $Ni_{1-x}Zn_xO$ cubic rocksalt solid solutions, Dalt. Trans. **44**, 14793 (2015).

[25] L. Gerward and J. S. Olsen, The high-pressure phase of zincite, J. Synchrotron Radiat. **2**, 233 (1995).

[26] R. D. Shannon, Revised effective ionic radii and systematic studies of interatomie distances in halides and chaleogenides, Acta Cryst. **A32**, 751 (1976).

[27] R. Schmidt, B. Rheinländer, M. Schubert, D. Spemann, T. Butz, J. Lenzner, E. M. Kaidashev, M. Lorenz, A. Rahm, H. C. Semmelhack, and M. Grundmann, Dielectric functions (1 to 5 EV) of wurtzite $Mg_xZn_{1-x}O$ ($0 \leq x < 0.29$) thin films, Appl. Phys. Lett. **82**, 2260 (2003).

[28] H. Yoshikawa and S. Adachi, Optical constants of ZnO, Jpn. J. Appl. Phys. **36**, 6237 (1997).

[29] M. D. Neumann, C. Cobet, N. Esser, B. Laumer, T. A. Wassner, M. Eickhoff, M. Feneberg, and R. Goldhahn, Optical properties of MgZnO alloys: Excitons and exciton-phonon complexes, J. Appl. Phys. **110**, 013520 (2011).

[30] S. Shokhovets, L. Spieß, and G. Gobsch, Spectroscopic ellipsometry of wurtzite ZnO and GaN: Examination of a special case, J. Appl. Phys. **107**, 023509 (2010).

[31] D. E. Aspnes, Approximate solution of ellipsometric equations for optically biaxial crystals, J. Opt. Soc. Am. **70**, 1275 (1980).

[32] J. H. Kang, Y. R. Park, and K. J. Kim, Spectroscopic ellipsometry study of $Zn_{1-x}Mg_xO$ thin films deposited on $Al_2O_3(0001)$, Solid State Commun. **115**, 127 (2000).

[33] M. Budde, C. Tschammer, P. Franz, J. Feldl, M. Ramsteiner, R. Goldhahn, M. Feneberg, N. Barsan, A. Oprea, and O. Bierwagen, Structural, optical, and electrical properties of unintentionally doped NiO layers grown on MgO by plasma-assisted molecular beam epitaxy, J. Appl. Phys. **123**, 195301 (2018).

[34] G. Jellison and L. Boatner, Optical functions of uniaxial ZnO determined by generalized ellipsometry, Phys. Rev. B **58**, 3586 (1998).

[35] J. F. Muth, R. M. Kolbas, A. K. Sharma, S. Oktyabrsky, and J. Narayan, Excitonic structure and absorption coefficient measurements of ZnO single crystal epitaxial films deposited by pulsed laser deposition, J. Appl. Phys. **85**, 7884 (1999).

[36] M. Wełna, R. Kudrawiec, A. Kaminska, A. Kozanecki, B. Laumer, M. Eickhoff, and J. Misiewicz, Contactless electroreflectance studies of free exciton binding energy in $Zn_{1-x}Mg_xO$ epilayers, Appl. Phys. Lett. **103**, 251908 (2013).

[37] T. Aoki and S. Adachi, Temperature dependence of the dielectric function of Si, J. Appl. Phys. **69**, 1574 (1991).

[38] R. Newman and R. Chrenko, Optical properties of nickel oxide, Phys. Rev. **114**, 1507 (1959).

[39] M. Ono, K. Sasaki, H. Nagai, T. Yamaguchi, M. Higashiwaki, A. Kuramata, S. Yamakoshi, M. Sato, T. Honda, and T. Onuma, Relation between electrical and optical properties of p-type NiO films, Phys. Status Solidi (b) **255**, 1700311 (2018).

[40] C. P. Liu, K. O. Egbo, C. Y. Ho, J. A. Zapien, W. Walukiewicz, and K. M. Yu, Stoichiometry Controlled Bipolar Conductivity in Nanocrystalline $Ni_xCd_{1-x}O_{1+\delta}$ Thin Films, Phys. Rev. Appl. **11**, 014019 (2019).

[41] S. Lany, J. Osorio-Guillén, and A. Zunger, Origins of the doping asymmetry in oxides: Hole doping in NiO versus electron doping in ZnO, Phys. Rev. B **75**, 241203(R) (2007).

[42] M. León, S. Levcenko, A. Nateprov, A. Nicorici, J. M. Merino, R. Serna, and E. Arushanov, Dielectric functions and fundamental band gaps of $Cu_2In_4Se_7$, $CuGa_3Se_5$ and $CuGa_5Se_8$ crystals, J. Phys. D. Appl. Phys. **40**, 740 (2007).

[43] P. Lautenschlager, M. Garriaga, S. Logothetidis, and M. Cardona, Interband critical points of GaAs and their temperature dependence, Phys. Rev. B **35**, 9174 (1987).

[44] C. P. Liu, Y. Foo, M. Kamruzzaman, C. Y. Ho, J. A. Zapien, W. Zhu, Y. J. Li, W. Walukiewicz, and K. M. Yu, Effects of Free Carriers on the Optical Properties of Doped CdO for Full-Spectrum Photovoltaics, Phys. Rev. Appl. **6**, 064018 (2016).

[45] J. Huso, L. Bergman, and M. D. McCluskey, Bandgap of cubic $ZnS_{1-x}O_x$ from optical transmission spectroscopy, J. Appl. Phys. **125**, 075704 (2019).

[46] B. D. Viezbicke, S. Patel, B. E. Davis, and D. P. Birnie, Evaluation of the tauc method for optical absorption edge determination: ZnO thin films as a model system, Phys. Status Solidi (b) **252**, 1700 (2015).

[47] A. Segura, J. A. Sans, F. J. Manjón, A. Muñoz, and M. J. Herrera-Cabrera, Optical properties and electronic structure of rock-salt ZnO under pressure, Appl. Phys. Lett. **83**, 278 (2003).

[48] M. A. Green and M. J. Keevers, Optical properties of intrinsic silicon at 300 K, Prog. Photovoltaics Res. Appl. **3**, 189 (1995).

[49] K. Bücher, J. Bruns, and H. G. Wagemann, Absorption coefficient of silicon: An assessment of measurements and the simulation of temperature variation, J. Appl. Phys. **75**, 1127 (1994).

[50] A. Ghosh, C. M. Nelson, L. S. Abdallah, and S. Zollner, Optical constants and band structure of trigonal NiO, J. Vac. Sci. Technol. A **33**, 061203 (2015).

[51] S. Logothetidis, P. Lautenschlager, and M. Cardona, Temperature dependence of the dielectric function and the interband critical points in orthorhombic GeS, Phys. Rev. B **33**, 1110 (1986).

[52] J. Y. Zhang, W. W. Li, R. L. Z. Hoye, J. L. MacManus-Driscoll, M. Budde, O. Bierwagen, L. Wang, Y. Du, M. J. Wahila, L. F. J. Piper, T. L. Lee, H. J. Edwards, V. R. Dhanak, and K. H. L. Zhang, Electronic and transport properties of Li-doped NiO epitaxial thin films, J. Mater. Chem. C **6**, 2275 (2018).

[53] N. Miller, J. W. Ager, H. M. Smith, M. A. Mayer, K. M. Yu, E. E. Haller, W. Walukiewicz, W. J. Schaff, C. Gallinat, G. Koblmüller, and J. S. Speck, Hole transport and photoluminescence in Mg-doped InN, J. Appl. Phys. **107**, 113712 (2010).

[54] H. Sato, T. Minami, S. Takata, and T. Yamada, Transparent conducting p-type NiO thin films prepared by magnetron sputtering, Thin Solid Films **236**, 27 (1993).

[55] H. J. va. Daal and A. Bosman, Hall effec in CoO, NiO, and α-Fe_2O_3, Phys. Rev. **158**, 736 (1967).

[56] F. A. Kroger and H. J. Vink, Relation between the concentrations of imperfections in crystalline solids, Solid State Phys. **3**, 307 (1956).

[57] P. Lunkenheimer, A. Loidl, C. R. Ottermann, and K. Bange, Correlated barrier hopping in NiO films, Phys. Rev. B **44**, 5927 (1991).

[58] A. Banerjee, S. Pal, and B. K. Chaudhuri, Nature of small-polaron hopping conduction and the effect of Cr doping on the transport properties of rare-earth manganite $La_{0.5}Pb_{0.5}Mn_{1-x}Cr_xO_3$, J. Chem. Phys. **115**, 1550 (2001).

[59] R. Karsthof, M. Grundmann, M. A. Anton, and F. Kremer, Polaronic inter-acceptor hopping transport in intrinsically doped nickel oxide, Phys. Rev. B **99**, 235201 (2019).

[60] J. Osorio-Guillén, S. Lany, and A. Zunger, Nonstoichiometry and hole doping in NiO, AIP Conf. Proc. 1199, 128 (2009).

[61] R. Al-Gaashani, S. Radiman, A. R. Daud, N. Tabet, and Y. Al-Douri, XPS and optical studies of different morphologies of ZnO nanostructures prepared by microwave methods, Ceram. Int. **39**, 2283 (2013).

[62] M. C. Biesinger, B. P. Payne, L. W. M. Lau, A. Gerson, and R. S. C. Smart, X-Ray photoelectron spectroscopic chemical state quantification of mixed nickel metal,

oxide and hydroxide systems, Surf. Interface Anal. **41**, 324 (2009).

[63] P. T. Hsieh, Y. C. Chen, K. S. Kao, and C. M. Wang, Luminescence mechanism of ZnO thin film investigated by XPS measurement, Appl. Phys. A **90**, 317 (2008).

[64] M. Taguchi, M. Matsunami, Y. Ishida, R. Eguchi, A. Chainani, Y. Takata, M. Yabashi, K. Tamasaku, Y. Nishino, T. Ishikawa, Y. Senba, H. Ohashi, and S. Shin, Revisiting the Valence-Band and Core-Level Photoemission Spectra of NiO, Phys. Rev. Lett. **100**, 206401 (2008).

[65] Y. Chen, O. Sakata, R. Yamauchi, A. Yang, L. S. R. Kumara, C. Song, N. Palina, M. Taguchi, T. Ina, Y. Katsuya, H. Daimon, A. Matsuda, and M. Yoshimoto, Lattice distortion and electronic structure of magnesium-doped nickel oxide epitaxial thin films, Phys. Rev. B **95**, 245301 (2017).

[66] A. R. González-Elipe, J. P. Holgado, R. Alvarez, and G. Munuera, Use of factor analysis and XPS to study defective nickel oxide, J. Phys. Chem. **96**, 3080 (1992).

[67] D. Tahir and S. Tougaard, Electronic and optical properties of Cu, CuO and Cu_2O studied by electron spectroscopy, J. Phys.: Condens. Matter **24**, 175002 (2012).

[68] W. Chen, Y. Wu, J. Fan, A. B. Djurišić, F. Liu, H. W. Tam, A. Ng, C. Surya, W. K. Chan, D. Wang, and Z. B. He, Understanding the doping effect on NiO: Toward high-performance inverted perovskite solar cells, Adv. Energy Mater. **8**, 1703519 (2018).

[69] J. R. Harwell, T. K. Baikie, I. D. Baikie, J. L. Payne, C. Ni, J. T. S. Irvine, G. A. Turnbull, and I. D. W. Samuel, Probing the energy levels of perovskite solar cells via kelvin probe aind UV ambinent pressure photoemission spectroscopy, Phys. Chem. Chem. Phys. **18**, 19738 (2016).

[70] W. Walukiewicz, Mechanism of Fermi-level stabilization in semiconductors, Phys. Rev. B **37**, 4760 (1988).

[71] D. T. M. Speaks, K. M. Yu, S. S. Mao, E. E. Haller, and W. Walukiewicz, Fermi level stabilization energy in cadmium oxide, J. Appl. Phys. **107**, 113706 (2010).

[72] D. M. Detert, K. B. Tom, C. Battaglia, J. D. Denlinger, S. H. N. Lim, A. Javely, A. Anders, O. D. Dubon, K. M. Yu, and W. Walukiewicz, Fermi level stabilization and band edge energies in $Cd_xZn_{1-x}O$ alloys, J. Appl. Phys. **115**, 233708 (2014).